ISSN 1063-7826, Semiconductors, 2009, Vol. 43, No. 3, pp. 331–339. © Pleiades Publishing, Ltd., 2009.
Original Russian Text © J.N. Kulchin, V.P. Dzyuba, A.V. Shcherbakov, 2009, published in Fizika i Tekhnika Poluprovodnikov, 2009, Vol. 43, No. 3, pp. 349–356.

LOW-DIMENSIONAL SYSTEMS

Optical Transmittance Spectra of Insulator Nanoparticles in Bulk Heterocomposites

J. N. Kulchin^, V. P. Dzyuba^^, and A. V. Shcherbakov

Institute of Automation and Control Processes, Far East Division, Russian Academy of Sciences, Vladivostok, 690041 Russia

^e-mail: kulchin@iacp.dvo.ru

^^e-mail: vdzyuba@iacp.dvo.ru

Submitted June 9, 2008; accepted for publication June 9, 2008

Abstract—A theoretical model is presented of the visible, near-infrared, and near-ultraviolet transmittance spectra of arbitrarily-shaped small-sized insulator particles embedded in an insulator in relation to the particle dimensions and the radiation frequency. The model is based on a number of assumptions. In the band gap of the nanoparticles, there are allowed energy bands produced by surface defects. Two-particle states (electron–hole pairs) are only slightly confined, and the size-quantized states of charge carriers are formed in the conduction band; the states depend on the shape and dimensions of the nanoparticles. By the example of Al_2O_3 nanoparticles introduced into a liquid matrix of a transparent insulator, the results of experimental studies are compared with the theoretical model.

PACS numbers: 73.22.-f, 78.20.Bh, 78.67.Hc, 81.07.Pr

DOI: 10.1134/S1063782609030130

1. INTRODUCTION

In the last few years, small-sized semiconductor and insulator nanoparticles (quasi-zero-dimensional systems) have attracted the growing attention of researchers, since the physical properties of such systems radically differ from the properties of homogeneous bulk materials. Due to this difference, the systems are finding an ever increasing use in various optoelectronic devices [1–4] and other areas of natural science and medicine [5–8]. In this context, it is important to understand what physical processes control the optical and electrical properties of nanoparticles in an external electromagnetic field.

It is known that the differences between nanoparticles and bulk samples in optical and electrical properties arise from differences in electron spectra [9–12]. These differences are due to a number of effects. First, in nanoparticles, the regions of allowed energies of charge carriers are formed in the band gap, with the structure controlled by a high density of surface defects of the crystal structure and by the irregular shape of the nanoparticles [13]. Second, nanoparticles exhibit the size-quantization effect responsible for the discrete energy spectrum in the conduction band and for the exciton energy spectrum modified by spatial confinement of the exciton wave functions [10, 12, 14–16]. Third, in such quasi-zero-dimensional systems, the electric dipole moments of transitions can take on large values that exceed the values typical of bulk samples [17]. The formation of the size-quantized states is of threshold character, depending on the nanoparticle's size. Specifically, in accordance with [18–23], such states are possible for a spherical particle with the permittivity ε_2 in a medium with the permittivity ε_1, if the nanoparticle's radius a is smaller than a certain critical radius a_c:

$$a \le a_c = 6|\beta|^{-1} a_{e,h}.$$

Here,

$$\beta = \frac{\varepsilon_1 - \varepsilon_2}{\varepsilon_1 + \varepsilon_2},$$

and a_e and a_h are the Bohr radii of an electron and a hole in the material of the nanoparticle.

One of the most important informative optical characteristics of the electronic structure and physical mechanisms controlling the optical and electrical properties of nanoparticles is presented by the transmittance and absorption spectra of an ensemble of nanoparticles in the near-infrared (IR) and near-ultraviolet (UV) regions [24]. However, at the present time, there are no studies, in which experimental investigations are combined with the theoretical description of the transmittance spectra of three-dimensional (3D) ensembles of small-sized insulator nanoparticles. As a rule, the transmittance spectra were experimentally studied for arrays of nanoparticles embedded into the bulk of a solid matrix or deposited onto the surface of a transparent material [11, 13, 25–27]. In such cases, the electronic structure of nanoparticles is substantially influenced by the material of the matrix, and if the nanoparticles are at the surface, their electronic structure is influenced by their interaction. For these reasons, it is impossible to consider the experimentally recorded transmittance and absorption spectra as the spectra of the arrays of noninteracting nanoparticles. A small number of theoretical studies are concerned with the development of the the-

ory of interaction of the electromagnetic field with one-particle states of charge carriers inside a spherically shaped semiconductor particle [9, 10].

The purpose of this study is to develop a theoretical model of the optical transmittance spectrum of an array of small-sized ($a < a_c$) noninteracting insulator nanoparticles embedded in an insulator matrix and to investigate the spectrum experimentally. In this study, we present a theoretical model of the transmittance spectrum in the visible and near-IR and near-UV regions. The experimental results are correlated with the theoretical model, using the 3D array of Al_2O_3 nanoparticles as an example.

The study involves a certain sequence of stages. At first, we derived the model's theoretical expressions that describe how the transmittance spectrum of a 3D array of insulator nanoparticles depends on their dimensions and the radiation frequency. The energy spectrum of charge carriers was theoretically studied for the Al_2O_3 nanoparticles. The derived relations served as a basis for the model's expressions describing the transmittance spectrum in different radiation frequency regions. The transmittance spectrum of the array of Al_2O_3 nanoparticles was experimentally studied by the standard technique with the use of a Hitachi U2010 spectrophotometer. Then, the theoretical and experimental transmittance spectra were compared.

2. BASIC RELATIONS

Let there be an ensemble of identically shaped insulator nanoparticles uniformly distributed in a matrix of a liquid insulator, and let their concentration be such that the interaction between the nanoparticles can be disregarded. In the case of a normal incidence of a beam of light, the transmittance T of a planar layer of such nanocomposite with the thickness h larger than the light's wavelength λ is represented as a function of the light frequency ω, the typical nanoparticle dimension a, and the number of particle per unit volume N by the expression [24]

$$T(\omega, a, N) = \frac{(1-R^2)^2\exp(-\alpha h)}{1-R^2\exp(-2\alpha h)}. \quad (1)$$

Here, R is the coefficient of optical reflection from the layer's boundary; in experiments, the reflectance R is, as a rule, much smaller than unity. The extinction coefficient α is expressed in terms of the cross section of optical scattering $\sigma_s(\omega, a)$ and the cross section of optical absorption $\sigma_a(\omega, a)$ of the nanoparticles:

$$\alpha = N[\sigma_a(\omega, a) + \sigma_s(\omega, a)] + \alpha_m(\omega).$$

Here, $\alpha_m(\omega)$ is the extinction coefficient of the matrix and N is the number of nanoparticles per unit volume [24]. The cross sections $\sigma_s(\omega, a)$ and $\sigma_a(\omega, a)$ can be represented in terms of the polarizability of the unit volume of the nanoparticle $A(\omega, a)$ by the expressions taken from [24, 28]:

$$\sigma_a(\omega, a) = \frac{4\pi\omega}{c}V\mathrm{Im}A(\omega, a),$$
$$d\sigma_s(\omega, a) = \frac{\omega^4}{c^4}V^2|A(\omega, a)|^2\sin^2\theta d\Omega. \quad (2)$$

Here, V is the nanoparticle's volume, θ is the angle between the scattering direction and the electric-field's vector of the electromagnetic wave, and c is the speed of light in free space. If the nanoparticle's dimensions are small, the energy spectrum of free charge carriers (electrons and holes) in the nanoparticle is controlled basically by the Coulomb interaction between the carriers and by the spatial confinement of the quantization region (nanoparticle volume) [10, 23]. Let us assume that, along with the continuous energy spectrum of free charge carriers, there are discrete size-quantized levels in the conduction band. At room temperature, the discrete levels are slightly broadened, and the behavior of charge carriers occupying these levels in an external electric field is adequately described in the dipole approximation [29, 30]. In this approximation, the polarizability of the unit volume of the nanoparticle, $A(\omega, a)$, can be expressed in terms of the matrix elements of the electric dipole moments of transitions $D_{ij}(a)$ between the quantum states $|i\rangle$ and $|j\rangle$ [23, 29]:

$$A(\omega, a) = \frac{2}{V\hbar}\sum_{i,j}\frac{|D_{ij}(a)|^2(\omega_j^2-\omega^2)}{(\omega^2-\omega_j^2)^2+\omega^2\Gamma_j^2}\omega_j + i\sum_{i,j}\frac{|D_{ij}(a)|^2\Gamma_j}{(\omega^2-\omega_j^2)^2+\omega^2\Gamma_j^2}\omega\omega_j. \quad (3)$$

Here, summation is performed over all radiation-excited dipole transitions and charge carriers, ω_j is the frequency of the transition, Γ_j is the width of the excited level, and $\hbar$ is Planck's constant. From relations (2) and (3), we obtain the expressions for the scattering cross sections:

$$\sigma_a(\omega, a) = \frac{8\pi}{c\hbar}\sum_{i,j}\frac{|D_{ij}(a)|^2\omega_j\Gamma_j}{(\omega^2-\omega_j^2)^2+\omega^2\Gamma_j^2}\omega^2, \quad (4)$$

$$\sigma_s(\omega, a) = \frac{4P\omega^4}{c^4\hbar^2}\sum_{i,j}\sum_{i,k}\frac{|D_{ij}(a)|^2|D_{ik}(a)|^2\omega_j\omega_k[(\omega_j^2-\omega^2)(\omega_k^2-\omega^2)+\Gamma_j\Gamma_k\omega^2]}{[(\omega_k^2-\omega^2)^2+\omega^2\Gamma_k^2][(\omega_j^2-\omega^2)^2+\omega^2\Gamma_j^2]}. \quad (5)$$

Here,

$$P = \int_{4\pi} \sin^2\theta d\Omega.$$

The dependence of the cross sections on the nanoparticle's dimensions can be determined, if the relations between the quantities $D_{ij}(a)$, ω_j, and Γ_j are known. The matrix element of the dipole moment of the transition from the state $|i\rangle$ to the state $|j\rangle$ is [30]

$$D_{ij}(a) = \Lambda(\varepsilon_1, \varepsilon_2) e \langle j|\mathbf{r}\gamma|i\rangle.$$

Here, $\mathbf{r}$ is the vector's radius of the charge, γ is the polarization vector of the electromagnetic wave inducing this transition, and the factor $\Lambda(\varepsilon_1, \varepsilon_2)$ takes account of the effects of the nanoparticle's shape and the permittivities of the nanoparticle and its surroundings. Specifically, for a spherical nanoparticle, we have [28]

$$\Lambda(\varepsilon_1, \varepsilon_2) = \frac{3\varepsilon_1}{2\varepsilon_1 + \varepsilon_2}.$$

From the theorem of the mean of the definite integral [31] and from the normalization of the wave functions to unity, it follows that the matrix element is

$$D_{ij}(a) = \Lambda(\varepsilon_1, \varepsilon_2) e \Psi_{[j]}(\mathbf{r}_1)\Psi_{[i]}(\mathbf{r}_i)\int_V r\gamma dr = d_{ij}a. \quad (6)$$

Here, $\mathbf{r}_1$ is the radius of the vector of a particular point within the nanoparticle's volume V, i and j are the corresponding set of quantum numbers of the initial and final states, and the quantity d_{ij} is directly dependent on the nanoparticle's shape. The linear dependence of the matrix element on the nanoparticle's dimension $D_{ij}(a)$ is valid for a smaller than a_c; when a becomes comparable to or larger than a_c, it is necessary to take into account the polarization interaction of charge carriers with the charge induced at the interface between the media [18]. If the nanoparticle's dimensions are larger than a_c, the matrix element $D_{ij}(a)$ is almost independent of a, since D_{ij} is defined by the localization region of states involved in dipole transitions and these states only slightly depend on the nanoparticle's dimensions at $a > a_c$ [17]. In the case of transitions to the region of continuous states, the matrix element of such a transition is proportional to the delocalization region of charge carriers; i.e., it is proportional to a, as in the case of bound states. Therefore, for dipole transitions to bound states and to the states of the continuous energy spectrum, we can write

$$D^{q}_{ij}(a) = d^{q}_{ij}a, \quad D^{ex}_{ij}(a) = d^{ex}_{ij}a, \quad \text{and } D^{c}_{ij}(a) = a^{c}_{ij}a \quad (7)$$

for the transitions to the quantum-confined states $D^{q}_{ij}(a)$, exciton states $D^{ex}_{ij}(a)$ and states of the continuous spectrum $D^{c}_{ij}(a)$, respectively. If the width Γ_j of the excited jth level is only slightly dependent on j, the ratio between the scattering and absorption cross sections is

$$\frac{\sigma_s(\omega, a)}{\sigma_a(\omega, a)} \approx \frac{P\omega^3}{2\pi c^3 \hbar \Gamma}\sum_j |D_{ij}(a)|^2.$$

For nanoparticles with a = 10–100 nm, in the frequency range $\omega = 10^{13}$–10^{16} Hz, at $\Gamma = 10^9$ Hz, this ratio does not exceed 10^{-7}. Therefore, the scattering cross section can be omitted from the expression for the coefficient of the optical extinction.

To clarify the dependence of the frequency ω_j on a at transitions to quantum-confined and exciton states, we represent the nanoparticle as a 3D potential well that has infinitely high walls and a geometric shape identical to that of the nanoparticle. The energy of charge carriers in the quantum-confined states is defined by their kinetic energy, and, in accordance with the boundary conditions at the surface of the potential well, it is explicitly dependent on the nanoparticle's dimensions and shape. For the frequency of the transition, we can write

$$\omega_j = \frac{E_j}{\hbar} = \frac{\hbar\varphi_j^2}{2m_{e,h}a^2}\chi = \frac{c_j}{a^2}. \quad (8)$$

Here, φ_j are the roots of the Schrödinger equation for free electrons (holes) in the potential well, as determined from the conditions at the boundary of this well, m_e and m_h are the effective masses of an electron and a hole, and χ is a factor defined by the nanoparticle's shape. Specifically, for a spherical nanoparticle, χ is equal to unity [18]. In the nanoparticle's bulk, the excitons, whose dimensions are smaller than the nanoparticle's dimensions, are most stable. Therefore, it is reasonable to assume that the frequency ω_j at transitions to exciton states depends on the nanoparticle's shape more heavily than on the nanoparticle's dimensions. Using (4), (7), and (8), we obtain $\sigma_a(\omega, a)$ at the transitions of charge carriers to quantum-confined states,

$$\sigma^{q}_a(\omega, a) = \frac{8\pi}{c\hbar}\sum_{i,j}\frac{(d^{q}_{ij})^2 c_j \Gamma_j}{\left(\omega^2 - \frac{c_j^2}{a^4}\right)^2 + \omega^2\Gamma_j^2}\omega^2, \quad (9)$$

and to exciton states,

$$\sigma^{ex}_a(\omega, a) = \frac{8\pi}{c\hbar}\sum_{ij}\frac{(d^{ex}_{ij})^2 a^2 \omega_j \Gamma_j}{(\omega^2 - \omega_j^2)^2 + \omega^2\Gamma_j^2}\omega^2. \quad (10)$$

For transitions to the continuous spectrum with $\omega_j = \omega$, we have

$$\sigma^{c}_a(\omega, a) = \frac{8\pi}{c\hbar}\sum_{i,j}\frac{(d^{c}_{ij}a\omega)}{\Gamma_j}. \quad (11)$$

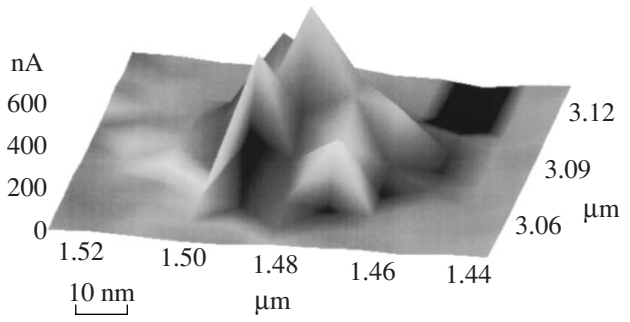

Fig. 1. Photograph of the AFM image of the Al_2O_3 nanoparticle.

Let us divide the frequency region in the vicinity of the absorption line with the central frequency ω_j into three regions: $\omega > \omega_j$, $\omega \approx \omega_j$, and $\omega < \omega_j$. If the quantities Γ_j are assumed to be independent of a, we obtain the expressions for the cross sections $\sigma_a^q(\omega, a)$ and $\sigma_a^{ex}(\omega, a)$ valid in the above three frequency regions. At $\omega > \omega_j$, we have

$$\sigma_a^q(\omega, a) \approx \frac{8\pi}{c\hbar}\sum_{i,j}\frac{(d_{ij}^q)^2 c_j\Gamma_j}{\omega^2} = A_1^q\omega^2,$$
$$\sigma_a^{ex}(\omega, a) \approx \frac{8\pi}{c\hbar}\sum_{j,j}\frac{(d_{ij}^{ex})^2 a^2\omega_j\Gamma_j}{\omega^2} = A_1^{ex}a^2\omega^2; \quad (12)$$

at $\omega = \omega_j$,

$$\sigma_a^q(\omega, a) \approx \frac{8\pi}{c\hbar}\sum_{i,j}\frac{(d_{ij}^q)^2 c_j}{\Gamma_j} = A_2^q,$$
$$\sigma_a^{ex}(\omega, a) \approx \frac{8\pi}{c\hbar}\sum_{j,j}\frac{(d_{ij}^{ex})^2 a^2\omega_j}{\Gamma_j} = A_2^{ex}a^2; \quad (13)$$

and at $\omega < \omega_j$,

$$\sigma_a^q(\omega, a) \approx \frac{8\pi}{c\hbar}\sum_{i,j}\frac{(d_{ij}^q)^2\Gamma_j a^8}{c_j^3}\omega^2 = A_3^q a^8\omega^2,$$
$$\sigma_a^{ex}(\omega, a) \approx \frac{8\pi}{c\hbar}\sum_{j,j}\frac{(d_{ij}^{ex})^2 a^2\omega^2\Gamma_j}{\omega_j^3} = A_3^{ex}a^2\omega^2. \quad (14)$$

For transitions to the states of the continuous energy spectrum in all frequency regions under discussion, we have

$$\sigma_a^c(\omega, a) \approx \frac{8\pi}{c\hbar}\sum_{j}\frac{(d_{ij}^c)^2 a\omega}{\Gamma_j} = A_1^c a\omega.$$

Taking into account (1), we obtain the transmittance spectrum of the array of nanoparticles as

$$T(\omega, a) \approx \exp[-Nh(A_1^q\omega^2 + A_2^{ex}a^2\omega^2 + A_1^c a\omega)] \quad (15)$$

at $\omega > \omega_j$ and

$$T(\omega, a) \approx \exp[-Nh(A_3^q a^8\omega^2 + A_3^{ex}a^2\omega^2 + A_1^c a\omega)] \quad (16)$$

at $\omega < \omega_j$. Introducing the quantity $\Delta\omega = \omega - \omega_j$, we obtain the transmittance

$$T(\omega, a) \approx \exp\left\{-Nh\sum_{ij}\left[\frac{(d_{ij}^q)c_j\Gamma_j}{4\Delta\omega^2 + \Gamma_j^2}\frac{(d_{ij}^{ex})^2\omega_j\Gamma_j a^2}{4\Delta\omega^2 + \Gamma_j^2} + A_1^c a\omega\right]\right\} \quad (17)$$

in the vicinity of the resonance frequency ω_j.

3. THE TRANSMITTANCE SPECTRUM: EXPERIMENTAL RESULTS

In the experiment, we studied the nanoparticles of the wide-gap aluminum oxide (Al_2O_3) insulator. According to the data of [32–34], the band gap of bulk aluminum oxide is wider than 6 eV, but narrower than 8.8 eV, and the refractive index is ~1.7. Nanoparticles with certain dimensions were separated from commercially manufactured nanopowders by elutriation in acetone. Figure 1 shows the photograph of the atomic force microscopy (AFM) image of Al_2O_3 nanoparticles precipitated from the suspension in acetone onto a polished silicon wafer. The AFM image was obtained with the use of an NT MDT Solver P46 atomic force microscope. The maximum average dimension across the nanoparticles was in the range from 40 to 50 nm. At the same time, the nanoparticle surface was not smooth, and some of the particles were shaped like irregular multipeak pyramids. These nanoparticles and a matrix of a transparent liquid insulator were used to produce a heterogeneous liquid-phase nanocomposite (HLPNC).

For the liquid matrix, we used the vacuum oil VM-4 (a colorless transparent viscous liquid with the refractive index ~1.4) that exhibits linear optical characteristics in the visible and IR spectral regions. The choice of the vacuum oil for the matrix was governed by the fact that, in the experimentally used regions of frequencies and light intensities, the resulting HLPNC is an optically linear medium. The interaction between nanoparticles was weak due to their low mass content in the HLPNC: the nanoparticle content was no higher than 0.03 wt %. The resulting HLPNC was placed into a cell made of an optical glass. The cell was shaped as a rectangular parallelepiped, with the thickness of the walls 160 μm; the width of the walls in the propagation direction of the light beam was 20 mm. In addition, we used a similar cell and pure vacuum oil to fabricate a reference sample of the planar transparent layer. The transmittance spectra of the HLPNC and reference sample were recorded with the use of a Hitachi U2010 spectrophotometer. By the standard method of dividing the transmittance spectrum of the HLPNC by the transmittance spectrum of the reference sample, we determined the transmittance spectrum of the ensemble of Al_2O_3

nanoparticles. Figure 2 shows the experimentally determined transmittance spectrum of the ensemble of Al_2O_3 nanoparticles (solid line). The wavelength's resolution was $\Delta\lambda = 0.5$ nm. The spectrum involves two moderately deep dips corresponding to two absorption bands in the ranges 220–225 and 265–307 nm and a relatively deep dip corresponding to the absorption band in the range 308–400 nm, with the minimum transmittances $T(\lambda = 237\ \text{nm}) = 0.425$, $T(\lambda = 287\ \text{nm}) = 0.445$, and $T(\lambda = 337\ \text{nm}) = 0.178$, respectively.

In the range 190–800 nm under consideration, the maximum transmittance is 0.88 and corresponds to $\lambda = 800$ nm. From Fig. 2, it is evident that, in the vicinity of the minimum of the transmittance spectrum in the range 308–400 nm, the dependence $T(\lambda)$ is asymmetric about the central wavelength $\lambda = 337$ nm. The long-wavelength part of the transmittance band is flatter and smoother than the short-wavelength part. The photon energy corresponding to the minimum transmittance at the wavelength $\lambda = 337$ nm is 3.7 eV, substantially smaller than the band gap E_g of the bulk crystal, but close to the $E_g = 3.6$ eV reported for the Al_2O_3 nanoparticles in [13]. The photon energies corresponding to the other two minima are 4.1 and 5.2 eV. The difference of these values from E_g of the bulk sample can be attributed to substantial changes in the electron structure of Al_2O_3 crystals, as their dimensions decrease to the nanoparticle's dimensions, and to the formation of extra allowed bands in the band gap. These extra bands can be produced by a large number of structural defects concentrated near the nanoparticle's surface, which is favored by the irregular shape of the nanoparticles (Fig. 1). It is the high concentration of defects near the nanoparticle's surface that is responsible for the formation of extra energy bands in the band gap of the material of the nanoparticles [13]. Then the energy $E_g = 3.7$ eV corresponds to the transition from the center of such band to the conduction band.

4. COMPARISON OF EXPERIMENTAL AND THEORETICAL RESULTS

The processes responsible for the transmittance spectrum are directly related to the energy spectrum of both free charge carriers and charge carriers bound in exciton pairs in the nanoparticle. Therefore, we estimate the energy spectrum of charge carriers for the Al_2O_3 nanoparticles studied in the experiment. Taking into account the spatial confinement of the wave functions of charge carriers in the nanoparticle's volume, we can assess the spectrum by modeling the nanoparticle by a system of charge carriers in an infinitely deep potential well, whose dimensions and shape are identical to those of the nanoparticle. To this end, we choose the model of the infinitely deep potential well confined by a paraboloid of revolution and by the dimensions of workable nanoparticles. The exciton binding energies in the spectrum are estimated by considering only the

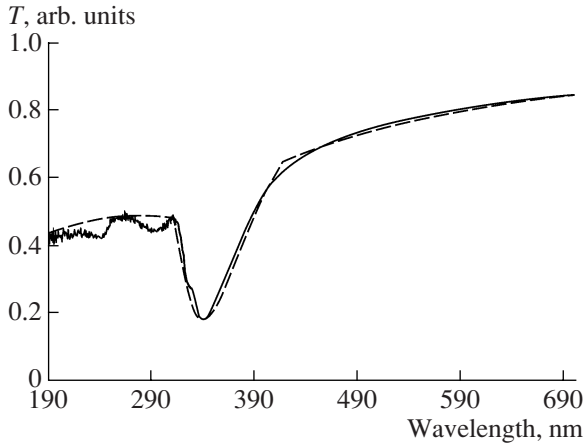

Fig. 2. The transmittance T of the array of Al_2O_3 nanoparticles versus the radiation wavelength λ. Solid and dashed lines show the experimental and simulated transmittance spectra, respectively. The wavelength resolution is $\Delta\lambda = 0.5$ nm. The content of Al_2O_3 nanoparticles in HLPNC is 0.01 wt %.

Coulomb electron–hole interaction and the size-quantization effect in the effective mass approximation, which proves to be correct for comparatively small nanoparticels [18–23]. The exciton wave function $\Psi(\eta, \xi, \varphi)$ in the parabolic coordinates with the origin at the center of mass of the electron–hole pair satisfies the equation [35]

$$\frac{4}{\xi\eta}\frac{\partial}{\partial\xi}\xi\frac{\partial\Psi}{\partial\xi} + \frac{\partial}{\partial\eta}\eta\frac{\partial\Psi}{\partial\eta} + \frac{1}{\xi\eta}\frac{\partial^2\Psi}{\partial\varphi^2} + 2\left(E + \frac{2}{\xi+\eta}\right) = 0. \quad (18)$$

In Eq. (18), we use relative units; i.e., Planck's constant and the charge are equal to unity; the electron's mass m_e, the hole's mass m_h and the exciton's mass

$$\mu = \frac{m_e m_h}{m_e + m_h}$$

are chosen in the effective mass approximation, and the unit's length is the exciton's Bohr radius in the material of the nanoparticle,

$$a_{\text{ex}} = \frac{\varepsilon_2}{\mu e^2}\eta^2.$$

The parabolic coordinates are related to the Cartesian coordinates by the following relations: $x = \sqrt{\xi\eta}\cos\varphi$, $y = \sqrt{\xi\eta}\sin\varphi$ and $z = \frac{1}{2}(\xi - \eta)$. The paraboloid of revolution about the $0z$ axis in the parabolic coordinates is defined by the equation $\eta = \eta_0$, and the plane $z = z_0$ corresponding to the nanoparticle's base is defined by the expression $\xi = 2z_0 + \eta$. The coordinates of the points at the nanoparticle's surface satisfy the two equations $\eta = \eta_0$ and $\xi = 2z_0 + \eta$. The condition of

the corresponding edge superimposed on the wave function at the surface of the potential well is

$$\Psi(\eta_0, \xi = 2z_0 = \eta, \varphi) = 0.$$

The solution of this problem, finite at the origin of coordinates and zero at infinity, is expressed in terms of degenerate hypergeometric functions $F(\alpha, |m| + 1, \rho)$ [35] as

$$\Psi(\eta, \xi, \varphi) = C\frac{1}{n^2|m|!}\sqrt{\frac{(a+|m|)!(\beta+|m|)!}{\alpha!\beta!}}$$
$$\times F\left(-\alpha, |m|+1, \frac{\xi}{n}\right)F\left(-\beta, |m|+1, \frac{\eta}{n}\right)$$
$$\times \exp\left(-\frac{\xi}{2n} - \frac{\eta}{2n} + im\varphi\right)\left(\frac{\xi\eta}{n^2}\right)^{|m|}.$$

The number n specifies the exciton's energy levels

$$E_n = \frac{\mu e^4}{2\varepsilon_2\eta^2 n^2}$$

and satisfies the relation $n = \alpha + \beta + |m| + 1$. The edge condition at the side surface of the paraboloid of revolution $\eta = \eta_0$ corresponds to the ground state, in which $\beta = 1$, $\alpha = 0$, and $n(|m| + 1) = \eta_0$. In this case,

$$n = \frac{|m|+1}{2} \pm \sqrt{\frac{(|m|+1)^2}{4} + \frac{\eta_0}{|m|+1}},$$

and each quantum number m corresponds to two energy levels. The value of $m = 0$ corresponds to the exciton moving in the plane parallel to the $0z$ axis. According to [32], the effective electron mass and hole mass in Al_2O_3 are $m_e = 0.4m_0$ and $m_h = 6.2m_0$, respectively. With these masses, for the nanoparticle with the height 40 nm and the base width 40 nm, the quantity η_0 expressed in relative units is 13, and, correspondingly, the energies of the exciton's ground state ($m = 0$) are –0.07 and –0.04 eV. Assuming that the kinetic energy of the exciton as a whole is negligible, we find that the exciton's energy levels are in the band gap at the energies 0.07 and 0.04 eV below the bottom of the conduction band. The second doublet of levels corresponding to $m = 1$ is moved away from the conduction band deep into the band gap by 0.05 and 0.21 eV. For $m = 2$, 3, and 4, the exciton's levels are, correspondingly, at 0.03 and 0.58 eV, 0.04 and 1.36 eV and 0.02 and 4.06 eV below the bottom of the conduction band. In the spectrum of these lines, one can notice the clearly pronounced effect of geometric amplification of the electron–hole interaction. The edge condition in the plane $\xi = 2z_0 + \eta$ corresponds to the excited state, for which $\beta = 0$, $\alpha = 1$, and

$$n = \frac{|m|+1}{2} \pm \sqrt{\frac{(|m|+1)^2}{4} + \frac{2z_0+\eta}{|m|+1}}.$$

In this state, the energy of the levels depends on the coordinate η that varies from zero to η_0. This dependence is representative of the effect of the shape of the potential well's surface on the exciton's energy spectrum. In general, the character of the exciton's energy spectrum remains the same as before. The spectrum consists of two regions, of which one is practically continuous and adjoined to the bottom of the conduction band from below, and the other is discrete and located deep in the band gap.

In the effective mass approximation, the wave function $\Psi(\eta, \xi, \varphi)$ written in the parabolic coordinates for a particle freely moving within the potential well satisfies Eq. (18) without the Coulomb term. The solution of this equation, finite at the origin of coordinates, is known and expressed in terms of the Bessel functions

$$\Psi(\eta, \xi, \varphi) = CJ_{m/2}\frac{k}{2}\eta J_{m/2}\frac{k}{2}\xi\exp(m\varphi).$$

The energy spectrum of a free particle is defined as

$$E_{n,m} = \frac{2\eta^2}{m_{e,h}}\frac{1}{\eta_0^2} + \frac{1}{(2z_0+\eta)^2}\alpha_{n,m}^2.$$

Here, $\alpha_{n,m}$ is the nth root of the Bessel function of the order $m/2$; the coordinates η_0 and z_0 are measured in nanometers. Similarly to the exciton's spectrum, the energy spectrum of free charge carriers depends on the variable η. Thus, taking into account the natural and thermal broadening of levels, we can state that the exciton's spectrum in the nanoparticles under consideration is formed by a practically continuous 0.1-eV-wide band adjoined to the bottom of the conduction band from below and by discrete levels localized deeply in the band gap at the energies 0.2 eV and larger below the bottom of the conduction band. The energy spectrum of charge carriers in the conduction band also can involve the discrete levels $E_{n,m}$.

The comparison of theoretical and experimental results is worthwhile in the regions of the absorption line and beyond it. The absorption line corresponds to the range $\lambda = 308$–400 nm that can be divided into the two ranges, $\lambda = 337$–400 nm and $\lambda = 308$–337 nm, in accordance with the particular mechanism of absorption. In the range $\lambda = 337$–400 nm, the mechanisms of excitation and decay of exciton states with the transitions of charge carriers into the conduction band are prevailing. In the range $\lambda = 308$–337 nm, the basic mechanisms are the transitions of charge carriers from the extra allowed energy bands arranged in the band gap to the conduction band.

To simulate the transmittance spectra numerically, expressions (15)–(17) were written as

$$T(\omega, a) \approx \exp[-(A_1\omega^2 + B_1\omega)], \quad \lambda \le 308 \text{ nm}, \tag{19}$$

$$T(\omega, a) \approx \exp[-(A_2\omega^2 + B_2\omega)], \quad \lambda > 400 \text{ nm}, \tag{20}$$

$$T(\omega, a) \approx \exp\left[-\left(\frac{A_3}{4\Delta\omega^2 + \Gamma_3^2}\right) + B_2\omega\right], \quad \lambda = 337\text{–}400 \text{ nm}, \tag{21}$$

$$T(\omega, a) \approx \exp\left[-\left(\frac{A_4}{4\Delta\omega^2 + \Gamma_4^2}\right) + B_4\omega\right], \quad \lambda = 308\text{–}337 \text{ nm}. \tag{22}$$

The experimentally measured transmittances corresponding to two radiation frequencies in each of the ranges $\lambda \approx 308$ nm and $\lambda > 400$ nm or to three frequencies in the ranges $\lambda = 337$–400 nm and $\lambda = 308$–337 nm were substituted into expressions (19)–(22) that then were considered as sets of equations in unknowns A, B, and Γ. The solutions of these sets of equations were substituted into expressions (19)–(22) in the corresponding regions. In this manner, we determined the model expressions for the particular transmittance spectra $T_m(\omega, a)$ to be compared with the experimentally determined transmittances. Figure 2 shows the experimental and model curves representing the dependences $T_m(\omega, a)$. Depending on the frequency region, model curves are plotted with the following values of A, B, and Γ:

$$A_1 = 1.09 \times 10^{31}, \quad B_1 = 7.239 \times 10^{17};$$

$$A_2 = 1.808 \times 10^{32} \text{ and } B_2 = 1.364 \times 10^{17};$$

$$A_3 = 2.733 \times 10^{30} \text{ and } \Gamma_3 = 1.258 \times 10^{15};$$

$$A_4 = 1.165 \times 10^{30} \text{ and } \Gamma_4 = 8.217 \times 10^{14};$$

$$B_3 = B_4 = 0.$$

As evident from Fig. 2, the experimental and model frequency dependences of the transmittance are in rather good agreement. The points of intersection of the experimental and theoretical curves correspond to the experimental transmittances used to construct the set of equations in unknowns A, B and Γ. In the experiment, we used the bulk nanocomposite containing nanoparticles similar in shape, but different in typical dimensions; the dimensions were in the range from 40 to 50 nm. Because of this, the transmittance spectrum of the nanocomposite is bound to involve broadened discrete lines. Depending on the quantity m for the exciton levels, their broadening can reach 0.04 eV for the levels adjoined to the bottom of the conduction band from below and 0.4 eV for the discrete levels in the band gap. These values are obtained in the case of a uniform size distribution of nanoparticels. The broadening of the lines of the energy spectrum of charge carriers in the conduction band can vary from 1 to 2 eV, depending on n and m. Therefore, the transmittance spectrum is described by a smoother curve than can be expected from the energy spectrum of charge carriers in an individual nanoparticle.

Let us now discuss the limits of applicability of the model suggested above. In deriving expressions (15)–(17), we assume that there exist energy levels of free charge carriers. Such levels are conditioned by spatial confinement of the quantization volume and by sufficient-long-lived excitons that make a noticeable contribution to the polarization of the nanoparticle. This requires that the nanoparticles be in the condition of weak confinement ($a^{ex} < a$). For the electron's (hole) energy levels $E_{n,m}$ to be formed due to spatial confinement of the quantization region, the energies $E_{n,m}$ must exceed the energy of interaction of charge carriers with the field $U(a)$ of polarization produced at the nanopartice–matrix interface. This interaction energy depends on the nanoparticle's shape and dimensions and on the dielectric properties of the medium surrounding the nanoparticle. Therefore, the determination of this energy for irregular asymmetric nanoparticles presents a nontrivial problem [10, 21–23]. To estimate this energy, we can make use of the expression given in [10] for a spherical particle of radius a,

$$U(a) \approx \frac{e^2\beta}{2\varepsilon_2 a},$$

where

$$\beta = \frac{\varepsilon_1 - \varepsilon_2}{\varepsilon_1 + \varepsilon_2}.$$

Then the condition for the formation of discrete energy levels due to spatial confinement of the quantization levels is

$$E_{n,m} \gg \frac{e^2\beta}{2\varepsilon_2 a}.$$

In the case of the above-considered nanoparticle with the height 40 nm and the base width 40 nm, this condition is satisfied. For example, with the electron's effective mass $0.4m_0$, the lowest electron levels are at the energies $E_{1,0} \approx 0.95$ eV and $E_{1,1} \approx 0.49$ eV, much larger than $U(a) \approx 10^{-3}$ eV for the 40 nm Al_2O_3 nanoparticle in the vacuum oil matrix. For nanoparticles embedded in an insulator medium, it is essential that the nanoparticle's dimension a should not exceed the threshold dimension $a_c = 6|\beta|^{-1}a_{e,h}$, where $a_{e,h}$ are the Bohr radii of an electron or a hole in the material of the nanoparticle [18–23].

5. CONCLUSIONS

It is known that the electronic structures of a small-sized insulator nanoparticle and the corresponding bulk material are radically different. This is manifested by the allowed energy regions formed in the band gap apparently due to surface defects and small dimensions

of the nanoparticle, by the changed energy of exciton states, and by the size- and shape-dependent size-quantized states of charge carriers in the conduction band of the nanoparticle.

The electric dipole moments of the transitions of charge carriers to both bound states and states of the continuous energy spectrum linearly depend on the nanoparticle's dimension, if this dimension does not exceed the threshold dimension a_c.

The cross section of optical scattering of the nanoparticle in the visible spectral region is seven orders of magnitude smaller than the absorption's cross section.

The frequency dependence of the absorption's cross section outside the absorption line is the same for the transitions of charge carriers to exciton states and size-quantized states. At frequencies above the absorption line, the absorption's cross section is inversely proportional to the frequency squared; below the absorption line, the absorption's cross section is proportional to the frequency squared. For transitions to the continuous spectrum, the absorption's cross section is proportional to the first power of the frequency at all frequencies.

The dependence of the absorption's cross section on the nanoparticle's dimension depends on the mechanism of optical absorption. In the case of absorption at the transitions of charge carriers to size-quantized states and at frequencies higher than or close to the resonance frequency, the absorption's cross section does not depend directly on the nanoparticle's dimension, but heavily depends on the nanoparticle's shape. At frequencies lower than the resonance frequency, the absorption's cross section is proportional to the eighth power of the typical nanoparticle dimension. For transitions to exciton states, the absorption's cross section is proportional to the square of the typical nanoparticle dimension; for transitions to the continuous spectrum, the absorption's cross section is proportional to the first power of the dimension at all frequencies.

The essential differences in the behavior of the absorption's cross section with the nanoparticle's dimension makes possible the experimental studies of the relative contributions of size-quantized and exciton states and the states of the continuous spectrum of charge carriers to the optical and electrical parameters of composite materials involving insulator nanoparticles.

ACKNOWLEDGMENTS

This study was supported in part by the Russian Foundation for Basic Research (project nos. 07-02-1442-a and 06-II-SO-02-005), and the program of fundamental studies of the Department of Physics of the Russian Academy of Sciences "Coherent Emission of Semiconductor Lasers and Structures".

REFERENCES

1. L. V. Asryan and R. S. Suris, Fiz. Tekh. Poluprovodn. **38**, 3 (2004) [Semiconductors **38**, 1 (2004)].
2. P. Michler, A. Kiraz, C. Becher, W. V. Schoenfeld, et al., Science **290**, 2282 (2000).
3. G. Yusa and H. Sakaki, Appl. Phys. Lett. **70**, 345 (1997).
4. E. Dekel, D. Gershoni, and E. Ehrenfreund, Phys. Rev. B **61**, 11009 (2000).
5. M. Brucher, M. Moronne, P. Gia, S. Weiss, and A. P. Alivisatos, Science **281**, 2013 (1998).
6. W. C. W. Chan and S. Nie, Science **281**, 2016 (1998).
7. M. Han, X. Gao, J. Su, and S. Nie, Nature Biotechnol. **19**, 631 (2001).
8. X. Michalet, F. F. Pihaud, and L. A. Betiolila, Science **301**, 538 (2005).
9. A. I. Belogorokhov, I. A. Belogorokhov, R. P. Miranda, and M. I. Vasilevsky, Zh. Éksp. Teor. Fiz. **130**, 123 (2007) [Phys. JETP **104**, 111 (2007)].
10. S. I. Pokutnyi, Fiz. Tekh. Poluprovodn. **40**, 233 (2006) [Semiconductors **40**, 217 (2006)].
11. V. S. Dneprovskii, E. A. Zhukov, E. A. Mulyarov, and S. P. Tikhodeev, Zh. Éksp. Teor. Fiz. **74**, 77 (2004).
12. Zh. I. Alferov, Fiz. Tekh. Poluprovodn. **32**, 3 (1998) [Semiconductors **32**, 1 (1998)].
13. O. P. Mikheeva and A. N. Sidorov, Zh. Tekh. Fiz. **74**, 77 (2004) [Tech. Phys. **49**, 739 (2004)].
14. Yu. V. Vandyshev, V. S. Dneprovskii, and V. I. Klimov, Pis'ma Zh. Éksp. Teor. Fiz. **53**, 301 (1991) [JETP Lett. **53**, 314 (1991)].
15. A. I. Ekimov, A. A. Onushchenko, and A. L. Efros, Pis'ma Zh. Éksp. Teor. Fiz. **43**, 292 (1986) [JETP Lett. **43**, 376 (1986)].
16. P. Dawson, E. O. Gwbel, and K. Pierz, J. Appl. Phys. **98**, 01354 (2005).
17. S. I. Pokutnii, Fiz. Tverd. Tela **39**, 720 (1997) [Phys. Solid State **35**, 634 (1997)].
18. N. A. Efremov and S. I. Pokutnii, Fiz. Tverd. Tela **27**, 48 (1985) [Sov. Phys. Solid State **27**, 27 (1985)].
19. N. A. Efremov and S. I. Pokutnii, Fiz. Tverd. Tela **32**, 2921 (1990) [Sov. Phys. Solid State **32**, 1697 (1990)].
20. N. A. Efremov and S. I. Pokutnii, Fiz. Tverd. Tela **33**, 2845 (1991) [Sov. Phys. Solid State **33**, 1607 (1991)].
21. S. I. Pokutnyi, Phys. Status Solidi B **165**, 109 (1991).
22. S. I. Pokutnyi, Phys. Status Solidi B **172**, 573 (1992).
23. S. I. Pokutnyi, Fiz. Tverd. Tela **35**, 257 (1993) [Phys. Solid State **35**, 129 (1993)].
24. C. Bohren and D. Huffman, *Absorbtion and Scattering of Light by Small Particles* (Wiley, New York, 1983; Mir, Moscow, 1986).
25. A. E. Zhukov, A. Yu. Egorov, A. R. Kovsh, et al., Fiz. Tekh. Poluprovodn. **31**, 104 (1997) [Semiconductors **31**, 84 (1997)].
26. V. P. Evtikhiev, I. V. Kudryavtsev, E. Yu. Kotel'nikov, et al., Fiz. Tekh. Poluprovodn. **32**, 1482 (1998) [Semiconductors **32**, 1323 (1998)].
27. S. V. Zaitsev, N. Yu. Gordeev, V. M. Ustinov, et al., Fiz. Tekh. Poluprovodn. **31**, 539 (1997) [Semiconductors **31**, 452 (1997)].

28. L. D. Landau and E. M. Lifshits *Course of Theoretical Physics*, Vol. 8: *Electrodynamics of Continuous Media* (Gostekhizdat, Moscow, 1957; Pergamon, New York, 1984).
29. V. M. Agranovich and V. L. Ginzburg, *Crystallooptics with the Account of Spatial Dispersion and Theory of Excitons* (Nauka, Moscow, 1979) [in Russian].
30. A. G. Davydov, *Quantum Mechanics* (Nauka, Moscow, 1982; Pergamon Press, New York, 1976).
31. G. Korn and T. Korn, *Mathematical Handbook for Scientists and Engineers* (McGraw-Hill, New York, 1967; Nauka, Moscow, 1973).
32. T. V. Perevalov, A. V. Shaposhnikov, V. A. Gritsenko, et al., Pis'ma Zh. Éksp. Teor. Fiz. **85**, 197 (2007) [JETP Lett. **85**, 165 (2007)].
33. M. I. Boltz and R. H. French, Appl. Phys. Lett. **55**, 1955 (1989).
34. M. Wakaki, K. Kudo, and T. Shibuya, *Physical Properties and Data of Optical Materials* (CRC Press, London, 2007).
35. L. D. Landau and E. M. Lifshits, *Course of Theoretical Physics*, Vol. 3: *Quantum Mechanics: Non-Relativistic Theory* (Nauka, Moscow, 1989, 4th ed.; Pergamon, New York, 1977, 3rd ed.).
36. É. Kalke, *Ordinary Differential Equations. A Reference Book* (Nauka, Moscow, 1976) [in Russian].

Translated by É. Smorgonskaya